Nuclear Physics A536 (1992) 648–668
North-Holland

NUCLEAR PHYSICS A

ULTRA-COLD ANTI-NEUTRONS (UCN̄)

(II). Production probability under magnetic and gravitational fields

H. YOSHIKI and R. GOLUB[1]

National Laboratory for High Energy Physics, Oho, Tsukuba-shi, Ibaraki-ken, 305, Japan

Received 30 April 1991

Abstract: The effects of wall collisions on an oscillating ultra-cold neutron-anti-neutron system can be partially compensated by an applied magnetic field. In this work we investigate this system in some detail based on the facts described in part I of this article using available n̄-nucleus potentials. We integrate over the UCN phase space including the effects of the earth's gravitational field.

1. Introduction

In part I of this article [1]) we established the validity of treating the problem of an nn̄ oscillating system (as proposed by Mohapatra and Marshak [2])) in a box by considering the particles as following classical trajectories contrary to the argument of Marsh and McVoy [3]). It was shown that, if the system is in the pure n state at $t=0$ the relative phase of n and n̄ is a "good number" even in the presence of wall collisions at least up to $\tau = Gt_c$, where t_c is the time between successive collisions and G, a measure of the gain of the proposed experiment, is defined in eq. (3.6) of this article. Since the suggestion of Mohapatra and Marshak [2]) concerning the possibility of nn̄ oscillations, there has been a growing interest in the experimental observation of such oscillations in free neutrons [4,5]).

The idea of carrying out such a search using ultra-cold neutrons (UCN) [6]), although inherently attractive because of the long storage times available with this technique (the probability of observing an anti-neutron grows proportional to t^2), has been rejected by most workers in this field [5]) because of the phase shifts and associated loss of coherence of the n̄-wave function as a result of collisions with the walls of the UCN container. However, one of the present authors has pointed out [7]) that it would be possible to compensate the n̄n relative phase shift caused by wall collisions with an opposite phase shift produced by an external magnetic field if coherence could be maintained.

It is the purpose of the present work to examine this suggestion in more detail. While it does not yet appear that an experiment using UCN is presently competitive

[1] Present address: Technical University Berlin, Germany.

with an experiment using cold neutrons, as described by Baldo-Ceolin [5]), the physics of the UCN-N̄ system is quite interesting, and the technology of UCN production is in rapid development with the possibility of future sources with significantly higher densities than are presently available [8,9]). In addition, as pointed out by Baldo-Ceolin [5]), if nn̄ oscillations are detected by another method, it may be possible eventually to use observation of UCN̄ as discussed in the present work, to obtain a high-precision determination of the n̄-matter interaction.

2. NN̄ oscillations in a magnetic field introduction of a geometrical model

The hamiltonian for the nn̄ system, in an external magnetic field in the case where nn̄ interactions exist can be written as

$$H = \begin{pmatrix} -\mu_0 B_0 & \varepsilon \\ \varepsilon & \mu_0 B_0 \end{pmatrix} \tag{2.1}$$

for n(n̄) with magnetic moment μ_0 parallel (anti-parallel) to the applied magnetic field. The diagonal terms are reversed in sign for the other spin state. In (2.1) the two basis states are n and n̄, respectively, and ε represents the transition mass between the two states violating the baryon number by two [2]). The probability of finding an n̄ at time t, starting with a pure n at time $t=0$ is

$$P_{n\bar{n}}(t) = \frac{\varepsilon^2}{\varepsilon^2 + (\mu_0 B_0)^2} \sin^2 \sqrt{(\mu_0 B_0)^2 + \varepsilon^2}\, t. \tag{2.2}$$

The phase diagram of this system is illustrated in fig. 1.

As is well-known [7,10]) eq. (2.2) shows that $P_{n\bar{n}}(t) = (\varepsilon t)^2$ for free oscillations ($B_0 = 0$, $\varepsilon t \ll 1$) as well as for $\omega_L t \ll 1$ (quasi-free oscillations) which imposes an

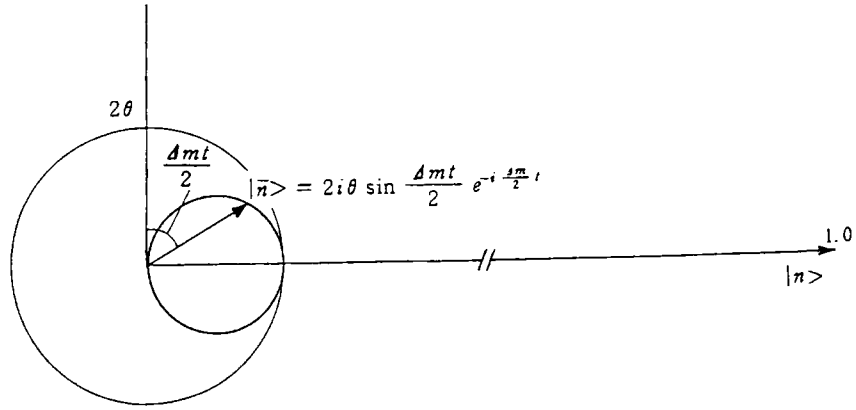

Fig. 1. Change of n̄ amplitude relative to n in the complex plane. The neutron moves freely in a magnetic field. $\Delta m = 2\sqrt{(\mu B)^2 + \varepsilon^2}$ as in eq. (2.2).

upper limit on the magnetic field which can be tolerated for a given observation time without loss of sensitivity to the $n\bar{n}$ oscillations. Several authors [10,11]) have shown that the effects of an external D-C field can be cancelled by simultaneous application of an oscillatory magnetic field. The idea is illustrated in fig. 1 of ref. [12]). Initially, the tip of the state vector in fig. 1 follows a circle, radius θ_0, centered at D with an angular velocity ω_L. If at $\omega_L t = \pi$ (when the vector is at C) we reverse the magnetic field, the center of motion moves to E$(-\theta)$ and at $\omega_L t = 2\pi$ the state vector is at F(-4θ). Another field reversal causes the state vector to precess in a "bootstrap" manner about point D again, so that at $\omega_L t = 3\pi$ we will be at a distance of 6θ from the origin. Successive field reversals will have the same action so that the distance from the origin increases by 4θ for every period $T = 2\pi/\omega_L$.

Thus we have

$$P_{n\bar{n}}(t) = (2/\pi)^2(\varepsilon t)^2 \tag{2.3}$$

or $(2/\pi)^2 = 0.63^2$ times the free-oscillation result. This can be compared to the value 0.58^2 obtained in ref. [11]) for the case of optimum sinusoidal modulation.

3. Effects of wall collisions on UCN–$\bar{N}$ oscillations

3.1. REFLECTION COEFFICIENT FOR UC$\bar{N}$

As is shown in part I [1]) of this paper, the semi-classical picture of the particle trajectories is valid for the values of observation time we discuss here. Therefore, our task of calculating the effect of a wall collision on the oscillations in the UCN-$\bar{N}$ system is reduced to knowing the s-wave scattering length for $\bar{n}$ on the nuclei present in the walls. As we are unaware of any direct measurement of this scattering length, or of the $\bar{n}$-nucleus optical potential, we will proceed in the same manner as previous authors who considered the effects of the strong interaction on the $n\bar{n}$ oscillations for neutrons bound in heavier nuclei [13]). That is, we will take the $\bar{n}$-nuclei potential to be that determined by fitting the observed hadronic contribution to the shifts and widths of energy levels in $\bar{p}$ atoms.

A recent analysis [14]) of the data for ^{12}C and ^{16}O - both materials having excellent reflection properties for UCN - finds that there is some ambiguity in this procedure, satisfactory fits being obtained with at least two different sets of potentials. One set (D) characterised by a deep absorptive potential and shallow real potential is similar to that obtained by other authors, while a second set(S) which has a shallow absorptive and a deep real part seems to give a better fit to the width of the excited state in the $\bar{p}$-atoms. Wong *et al.* [14]) take an optical potential whose shape is chosen to be similar to the nuclear density distribution as observed by electron scattering. We will use two model potentials in order to give some idea of the sensitivity of our results to the shape of the $\bar{n}$-nucleus potential. In our first model we simplify the potential to a square-well form with depth as given in ref. [14]), and radius equal

to the radius parameter of the diffuse shape taken there. Our second model will be a modified Fermi distribution which we will refer to as the "diffuse" potential.

For the square-well potential we have

$$U(r) = \begin{cases} -V - iW & r < R \\ 0 & r > R \end{cases} \tag{3.1}$$

with the parameters [14]) in the left part of table 1. Using the potential given by (3.1) the solution of the radial Schrödinger equation yields [15,16])

$$\tilde{a} = R(1 - \tan \tilde{k}R/\tilde{k}R) \tag{3.2}$$

for the s-wave scattering length, where the tilde indicates a complex quantity and

$$(\tilde{k})^2 = \frac{2M_r}{\hbar^2}(V + iW)\,. \tag{3.3}$$

M_r is the reduced mass.

For the diffuse potential we have numerically integrated the Schrödinger equation for the complex wave function and complex potential, starting at $r = 0$ continuing until the potential is negligibly small. We then rotate the resulting complex wave function until it has the form $c(r - a - ib)$ and identify $a + ib$ as the complex scattering length $\tilde{a}$. This procedure yields results in agreement with (3.2) and (3.3) for the square-well potential. The results for the diffuse potential along with the potential parameters given by Wong *et al.* [14]), following their notation, are shown in table 1.

The encounter of a UCN with a material wall is described by assuming the material-vacuum boundary is an infinitely sharp smooth surface, and the material is homogeneous [6]).

The wave vector for propagation of a UCN inside the wall is given by $\tilde{k}'$, where

$$(\tilde{k}')^2 = k_\perp^2 - 4\pi N\tilde{a} \tag{3.4}$$

where $k_\perp$ is the (real) wave vector of the incident neutron in vacuum in the direction perpendicular to the surface of the wall, N the number density of nuclei in the material, and $\tilde{a}$ the s-wave scattering length. For UC$\bar{N}$ we use $\tilde{a}$ as given in the

TABLE 1

Potential parameters taken from Wong *et al.* [14])

	V (MeV)	W (MeV)	R (fm)	w (fm)	a_V (fm)	a_w (fm)	square well $\tilde{a}$ (fm)	diffuse potential $\tilde{a}$ (fm)
^{12}C(S)	296	44	2.355	−0.149	0.548	0.527	2.488 − *i*0.2610	3.16 − *i*0.873
^{12}C(D)	127	119	2.355	−0.149	0.548	0.527	2.227 − *i*0.3299	3.11 − *i*1.10
^{16}O(S)	198	30	2.608	−0.051	0.539	0.518	2.548 − *i*0.6527	3.98 − *i*0.848
^{16}O(D)	86	161	2.608	−0.051	0.539	0.518	2.429 − *i*0.2976	3.50 − *i*0.948

table. The reflection coefficient $\tilde{R}$ is given by the ususal boundary conditions as [6])

$$\tilde{R} = \frac{k_\perp - \tilde{k}'}{k_\perp + \tilde{k}'} = \rho\, e^{i\varphi}, \tag{3.5}$$

and is thus a function of $k_\perp$ only. For UCN we use $a = 5.803$ fm for ^{16}O ($N = 0.5367 \times 10^{23}$) and $a = 6.648$ for ^{12}C ($N = 0.996 \times 10^{23}$). The results for UC$\bar{N}$ ($\rho_{\bar{n}}, \varphi_{\bar{n}}$) are plotted for ^{12}C in fig. 2a along with φ_n and $(\varphi_n - \varphi_{\bar{n}})$ for the different potential models while the results for ^{16}O are in fig. 2b. At these energies $\rho_n \sim 1 - \xi$ with $\xi < 10^{-3}$. Note that the differences between the S and D solutions are not very large. As expected, the reflection coefficient for UC$\bar{N}$ is considerably worse than for UCN. This is because of the relatively small real part of $\tilde{a}$ and the large imaginary part due to $\bar{n}$ annihilation. Even so, we see that a UC$\bar{N}$ can make several collisions before loss.

3.2. REFLECTION OF A UCN-$\bar{N}$ SYSTEM

This problem has already been dealt with in sects. 7 and 8 of ref. [12]). We add appendixes A and B in this paper to provide theorems and their proofs used in the

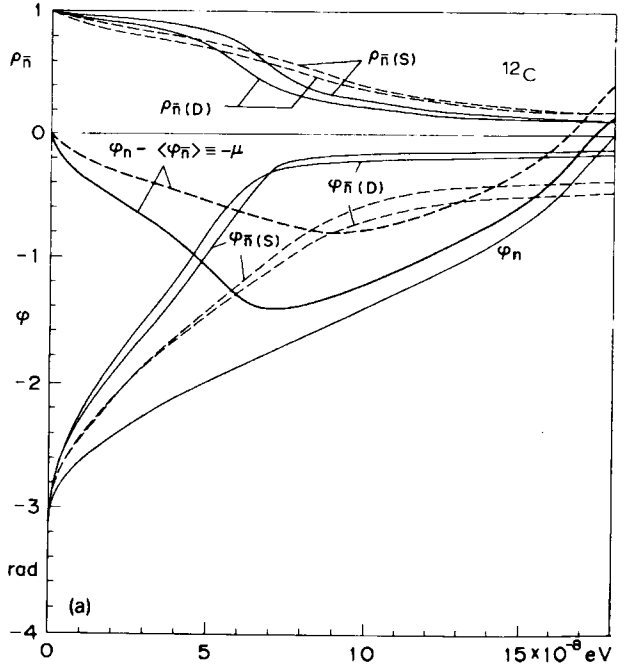

Fig. 2a. Reflectivity $\rho_{\bar{n}}$ and relative phase change $\varphi_n - \langle\varphi_{\bar{n}}\rangle$ due to a wall collision on carbon. The solid and dotted lines are for square-well and diffuse potential, respectively. See text for the explanation of S and D whose potential parameters are listed in table 1.

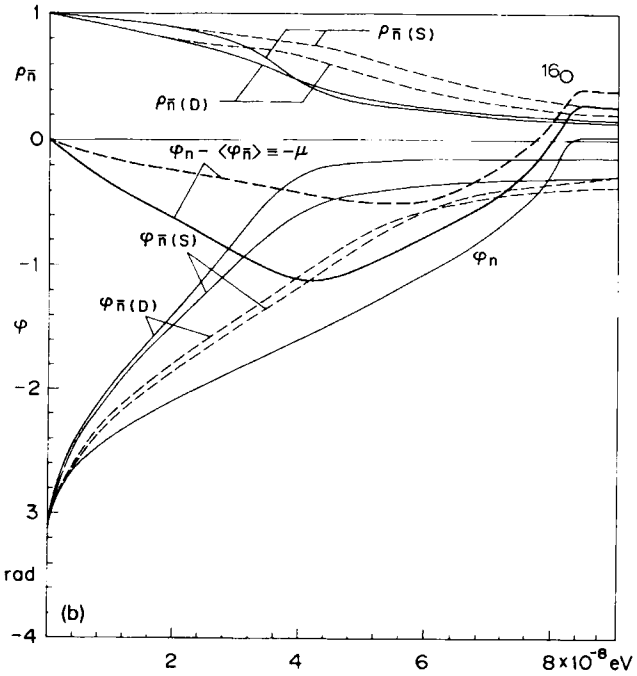

Fig. 2b. Reflectivity $\rho_{\bar{n}}$ and relative phase change $\varphi_n - \langle\varphi_{\bar{n}}\rangle$ due to a wall collision on oxygen. The solid and dotted lines are for square-well and diffuse potential, respectively. See text for the explanation of S and D whose potential parameters are listed in table 1.

argument. We define a parameter G, which will be a measure of the gain of the experiment by

$$G = \frac{4p}{\theta^2 \alpha^2} = \frac{1}{\alpha^2} \frac{4(1-\rho_{\bar{n}}^2)\sin^2 \tfrac{1}{2}\alpha}{1 + \rho_{\bar{n}}^2 - 2\rho_{\bar{n}} \cos(\mu - \alpha)}, \tag{3.6}$$

where

$$p = p_\infty$$

in eq. (4.3) and

$$\theta = \arctan(\varepsilon / \mu_0 B_0).$$

The effective coherence time τ of the experiment then will be

$$\tau = G t_c \tag{3.7}$$

where t_c is the time between the collisions, and τ is defined so that the probability

of observing an $\bar{n}$ during a time interval Δt after many collisions is

$$P_{\bar{n}} = \varepsilon^2 \Delta t \tau . \tag{3.8}$$

[See eqs. (17)-(19) of ref. [12])].

4. UCN–$\bar{N}$ oscillations in the absence of gravity

4.1. GEOMETRICAL CONSIDERATIONS

In order to concentrate on the essentials of the $n\bar{n}$ oscillating system we first consider the case where the earth's gravitation is absent. It seems that in this case the simplest geometry to consider is a spherical UCN cavity.

Considering only specular reflection, successive reflections of a single neutron always occur at the same angle with respect to the surface normal and hence with the same values of normal component of velocity of $\rho_{\bar{n}}$ and of $\mu = \varphi_{\bar{n}} - \varphi_n$. The distance between collisions is thus

$$z = 2r \cos \eta ,$$

where η is the incident angle. In fig. 3, we show $10 \ln G$ [eq. (3.6)] as a function of E and $\cos \eta$ for a sphere with radius $r = 0.3$ m and $B_0 = 3 \times 10^{-5}$ G calculated with the average of the reflectivities for the S and D square-well potentials. The resonance is seen to be very high and narrow.

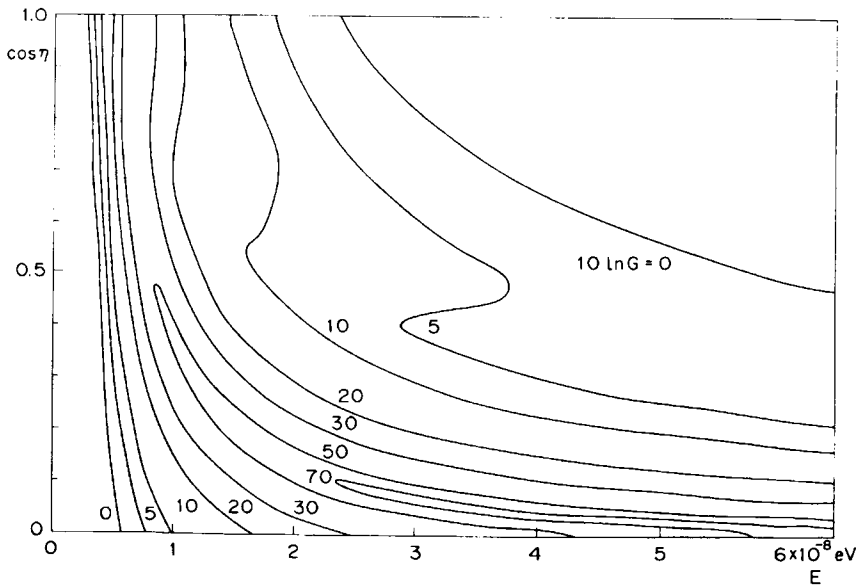

Fig. 3. Plot of $10 \ln G$ versus energy and $\cos \eta$ for a sphere with radius 0.3 m and $B_0 = 3 \times 10^{-5}$ G, square-well potential.

4.2. DETECTION OF THE $\bar{N}$

If one considers the total probability of an $\bar{n}$ annihilation up to the nth collision (assuming that all the annihilation products are detected in a surrounding detector bank), this probability can be calculated according to the following recurrence formula:

$$P_n = P_{n-1} + p_n , \tag{4.2}$$

where P_n is the total $\bar{n}$ annihilation probability up to the nth collision and

$$p_n = |b_n|^2 (1 - \rho_{\bar{n}}^2) \tag{4.3}$$

where $|b_n|$ is given by eq. (13) of ref. [12]). Note P_n increases by p_n after each collision. For a ^{12}C sphere of 60 cm diameter in a magnetic field of $B_0 = 2 \times 10^{-5}$G, fig. 4 shows the relation between $p_{n=100}$ of eq. (4.3), UC$\bar{N}$ energy and $\cos \eta$, θ being normalised to 1.

The peaks and shoulders of the curves reflect the resonances at $\mu = \alpha$ and their higher-order satellites in the interference pattern of the type shown in fig. 5.

When $\alpha = \mu$ for $n \to N$,

$$P_{n \to N} / \theta^2 \sin^2 \tfrac{1}{2}\alpha = \sum_{n=1}^{N} \left(\frac{1 - \rho_{\bar{n}}^n}{1 - \rho_{\bar{n}}} \right)^2 (1 - \rho_{\bar{n}}^2). \tag{4.4}$$

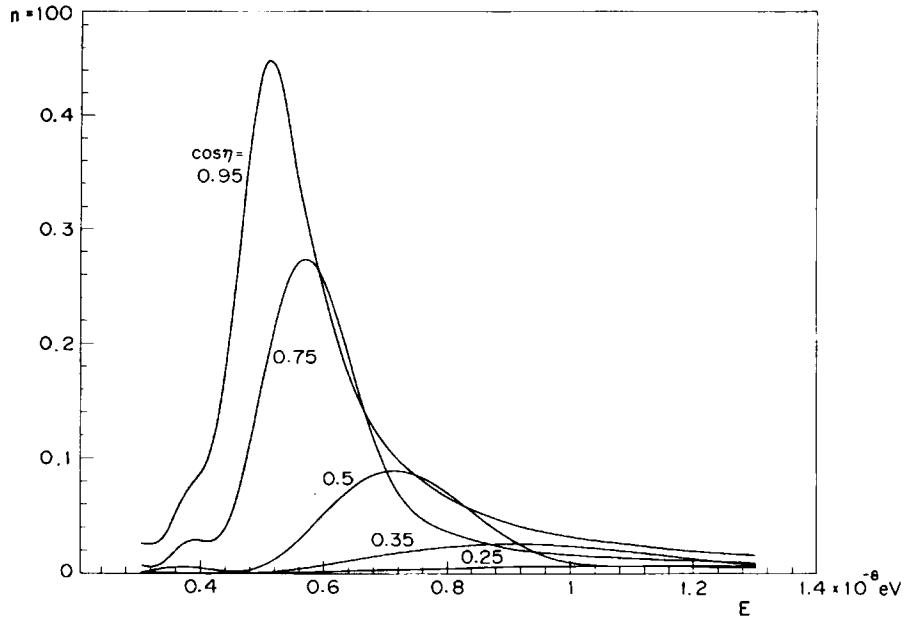

Fig. 4. $p_{n=100}$ of eq. (4.3) versus UC$\bar{N}$ energy for a ^{12}C sphere of radius 30 cm in $B_0 = 2 \times 10^{-5}$ G, square-well potential.

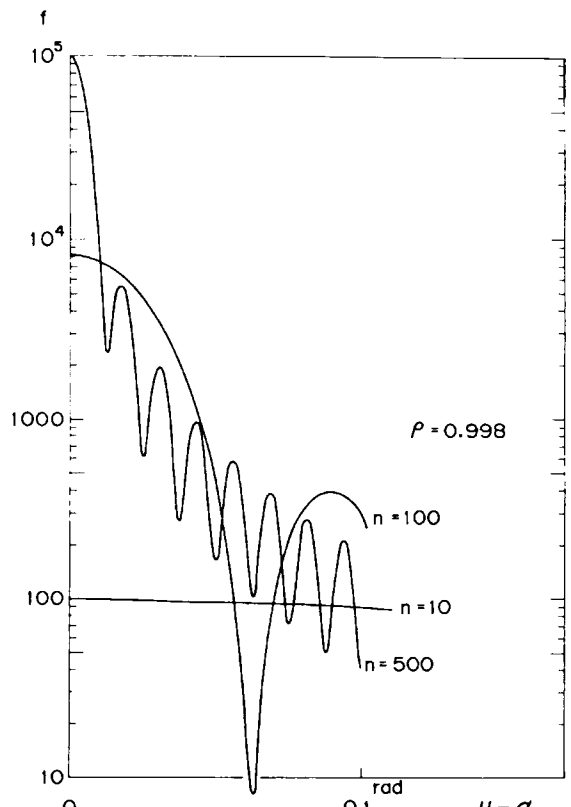

Fig. 5. Interference pattern of the function f (eq. (4.5)) with respect to $\mu-\alpha$, for $\rho_{\bar{n}}=0.998$.

The right-hand side of (4.4) is shown in fig. 6. One sees from fig. 2a that the contribution to $\bar{n}$ production is mainly from higher ρ-values, or smaller vertical UCN energies ($E_\perp \leq 4\times10^{-8}$ eV).

4.3. NUMERICAL INTEGRATION

To proceed further, it is necessary to make numerical integrations of P_n over E and η according to their probability distributions, $P(E)\,dE=\sqrt{E}\,dE$ and $P(\eta)\,d\eta=\cos\eta\,d(\cos\eta)$. Since, unlike ordinary gases, UCN are absorbed at the time of their contact with the wall with a certain probability, the $\cos\eta$ distribution is not strictly true, but this effect is small and neglected.

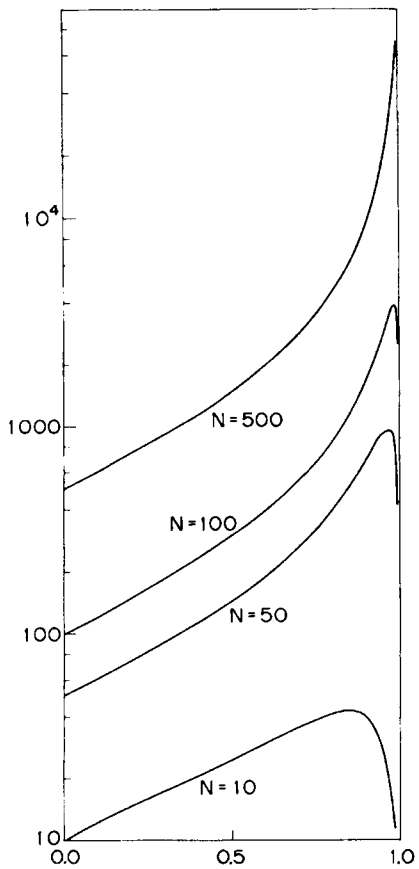

Fig. 6. Eq. (4.4) versus $\rho_{\bar{n}}$ for $N=10$, 50, 100 and 500.

The probability of detecting an $\bar{n}$ up to the Nth collision is [from eqs. (4.2), (4.3) and ref. [12]), eq. (13)]

$$P_{n\to N}=\sum_{n=1}^{N}\theta^2\,\frac{\int_0^1\int_0^{E_{max}}\sin^2\tfrac{1}{2}\alpha f(n,\mu,\alpha,\rho_{\bar{n}})(1-\rho_{\bar{n}}^2)\sqrt{E}\,dE\cos\eta\,d(\cos\eta)}{\int_0^1\int_0^{E_{max}}\sqrt{E}\,dE\cos\eta\,d(\cos\eta)}, \quad (4.5)$$

where

N = final number of collisions from the wall,

$\theta=\varepsilon/\mu_0 B_0$ = twice the usual mixing angle,

$\alpha = \alpha(E, \eta, B_0) = \omega_L t_c$,

$f(n, \mu, \alpha, \rho_{\bar{n}}) = (1+\rho_{\bar{n}}^{2n} - 2\rho_{\bar{n}}^{n} \cos(n(\mu-\alpha)))/(1+\rho_{\bar{n}}^2 - 2\rho_{\bar{n}} \cos(\mu-\alpha))$,

and $\mu = \mu(E, \eta)$ and $\rho = \rho(E, \eta)$ are calculated separately from fig. 2a. The integrations were performed using a mesh of 100 points for the E integration, and 20 points for the cos η integration. The maximum energy was 18×10^{-8} eV, the UCN cut-off energy for ^{12}C.

4.4. RESULTS FOR THE SPHERICAL GEOMETRY WITHOUT GRAVITY

In fig. 7 we show the total probability of detecting an $\bar{n}$ (per UCN) for a 100 s measuring time. We show the results for spherical radii $R = 0.3$ and 1.0 m as a function of applied magnetic field. We have taken the $n\bar{n}$ interaction strength $\varepsilon = 10^{-23}$ eV ($\tau_{n\bar{n}} = 6 \times 10^7$ s). The resonance at $\mu = \alpha$ is smeared out due to the

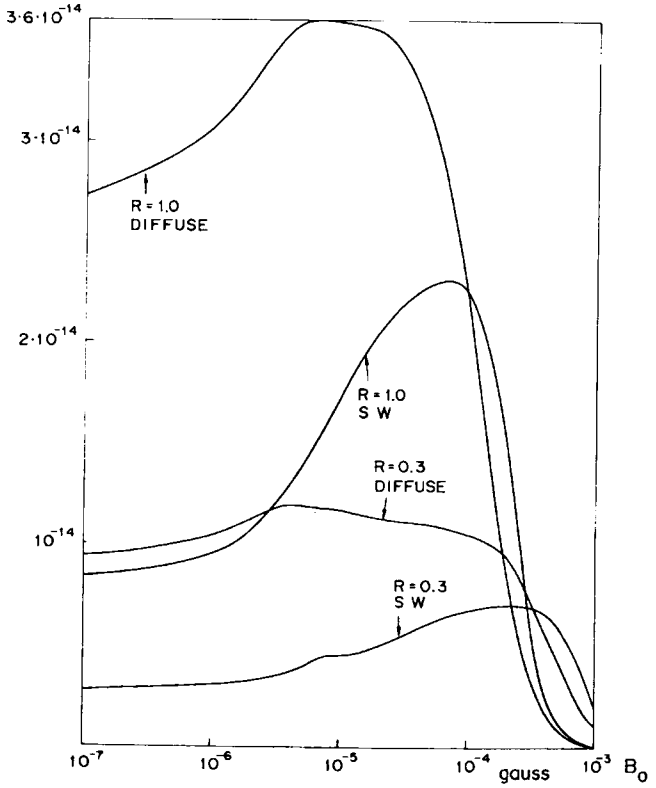

Fig. 7. Total probability of $\bar{n}$-annihilation in the first 100 s for a spherical ^{12}C container of radius R m neglecting gravity versus applied magnetic field for square-well and diffuse ^{12}C potential ($\varepsilon = 10^{-23}$ eV).

integration over the phase space. The overall probabilities are not insignificant, i.e. $1\text{-}3 \times 10^{-14}$. Results are shown for both the square-well and diffuse-potential shapes using the average of the reflectivities calculated from the S and D parameters of ref. [14]).

For comparison the result expected from a quasi-free experiment using meV neutrons and a flight time of 0.1 s would be an $\bar{n}$ probability of 2.5×10^{-18} per neutron using the above value of ε. (Presently available UCN throughputs are so small that the UCN experiment is not at all competitive using existing sources.)

For the 0.3 m radius sphere the average collision time (averaged over the phase space) is 0.07 s and the $\bar{n}$ probability is 1.2×10^{-14} (fig. 7). Using (3.6), (3.7) and (3.8) we find the effective average coherence time, τ, in the UCN case: (ΔT = UCN measuring time = 100 s, t_{qf} = flight time in quasi-free experiment = 0.1 s)

$$\frac{\tau \Delta T}{(t_{qf})^2} = \frac{1.2 \times 10^{-14}}{2.5 \times 10^{-18}},$$

$$\tau = 0.5 \text{ s},$$

or seven collision times.

5. Effect of gravity on UCN–$\bar{N}$ oscillations

5.1. KINEMATICS AND SELECTION OF GEOMETRY

The trajectories of particle motion in the earth's gravitational field are well-known to be parabolas. For neutrons moving upwards the maximum height attained by a given parabola can be written as

$$H = v_y^2/2g, \tag{5.1}$$

where g is the acceleration of gravity and

$$v_y = v \cos \eta \tag{5.2}$$

is the vertical component of velocity at the reference plane from which H is measured (fig. 8). The trajectory recrosses this reference plane after a time t_c:

$$t_c = 2v_y/g = 2v \cos \eta / g, \tag{5.3}$$

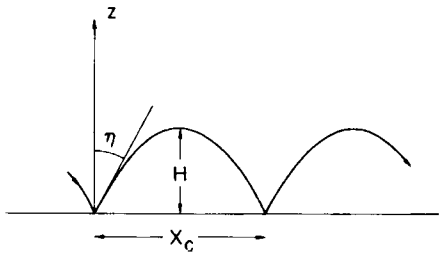

Fig. 8. Parabolic trajectory under influence of gravity.

when it will have travelled a horizontal distance

$$x_c = v_x t_c = 2v_x v_y / g = 2v^2 \sin\eta \cos\eta / g, \tag{5.4}$$

(v is the magnitude of the neutron velocity and η is the angle between the velocity and vertical direction - both taken at the reference plane). Hence we see that for UCN bouncing on a horizontal plane the behaviour of the UCN-$\bar{N}$ reflections will be completely determined by a single parameter, since both $\alpha = \omega_L t_c$ and μ are functions of the vertical velocity (or maxium height of the trajectory) only. Thus for a given magnetic field the entire phase space will lie on a single curve in the μ, α-plane as shown in fig. 9. This is quite different from the case without gravity where the time between collisions is inversely proportional to velocity and μ and α have a quite different dependence on the trajectory parameters. For the case of a sphere without gravity, the condition $\mu = \alpha$ restricts the phase space to a narrow range of energies. For the case including gravity fig. 9a shows that for $B = 4 \times 10^{-5}$ G the μ, α curve for the phase space remains in the vicinity of $\mu = \alpha$ for most of the effective energy range below the $\bar{n}$ cut off.

Of course, this favourable situation will be disrupted by the need to contain the neutrons in a finite region by vertical walls. Fig. 10 shows the horizontal component

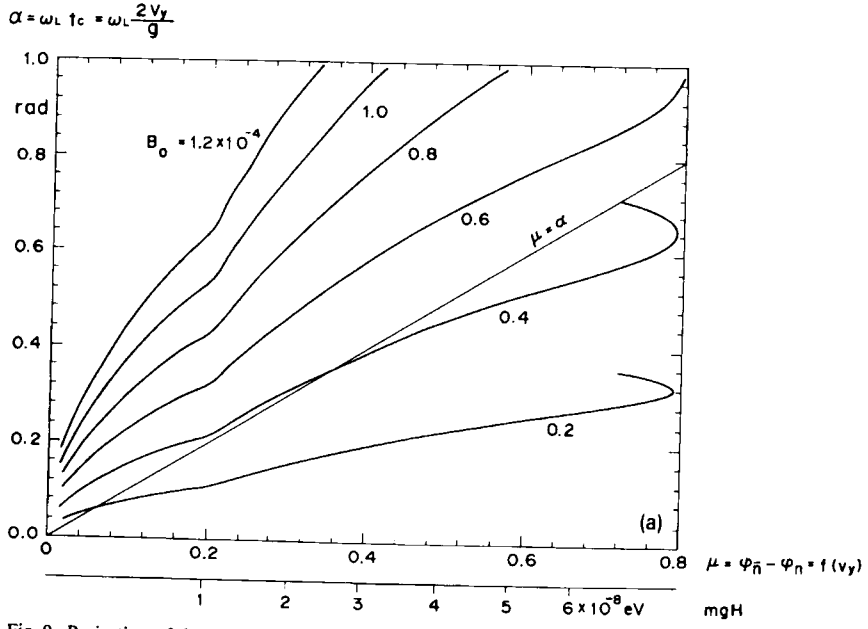

Fig. 9. Projection of the phase space onto the μ, α-plane for (a) the diffuse and (b) the square-well ^{12}C potential under the influence of gravity; collisions with a horizontal plane.

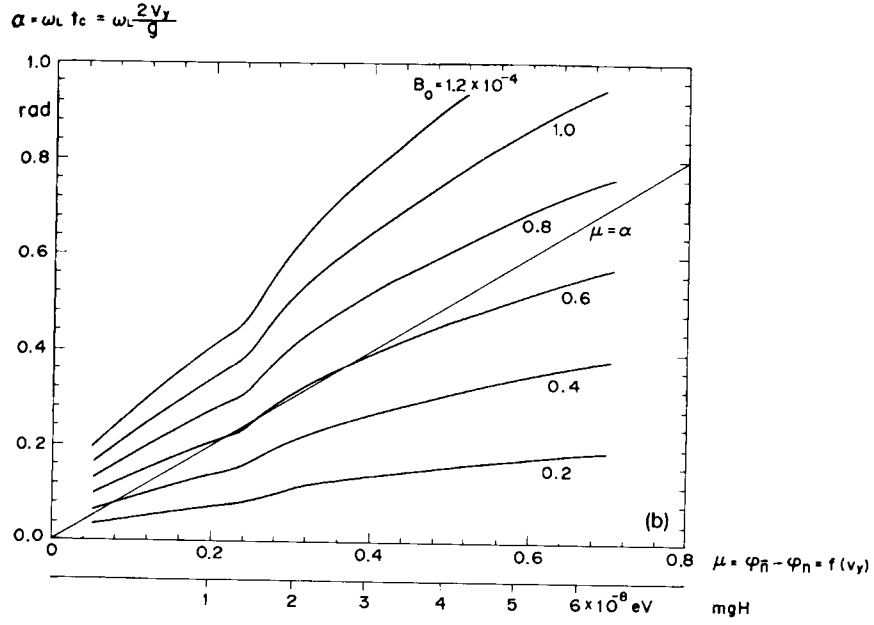

Fig. 9—continued.

of a trajectory moving in a vertical circular cylinder. The effect of a wall collision will depend on the horizontal velocity component, $v \sin\eta$, and the angle, ϕ, between this component and the normal to the wall at the point of collision.

5.2. EVOLUTION OF THE UCN-$\bar{N}$ SYSTEM-EFFECTS OF THE WALL COLLISIONS

As in sect. 4, we can trace the motion of the system point in the complex plane of fig. 1.

In fig. 11 we show trajectories for two values of magnetic field (all other trajectory parameters kept constant) neglecting the wall collisions. The results for the saturation points are in agreement with eq. (18) of ref. [12]). We see that in fig. 11b, the magnetic field is in resonance with the wall collisions and we reach the maximum amplitude. In fig. 12 we introduce the effects of wall collisions (radius of cylinder, $R = 0.3$ m) keeping all other parameters unchanged. In fig. 12b the field is the same (7.0×10^{-6} G) as that which produced a resonance condition in fig. 11b. The wall collisions produce an additional uncompensated the counter-clockwise rotation considerably reducing the saturation value of the $\bar{n}$ amplitude. In fig. 12b a larger magnetic field (1.3×10^{-5} G) compensates the counter-clockwise drift but only restores a part of the amplitude lost from fig. 11b.

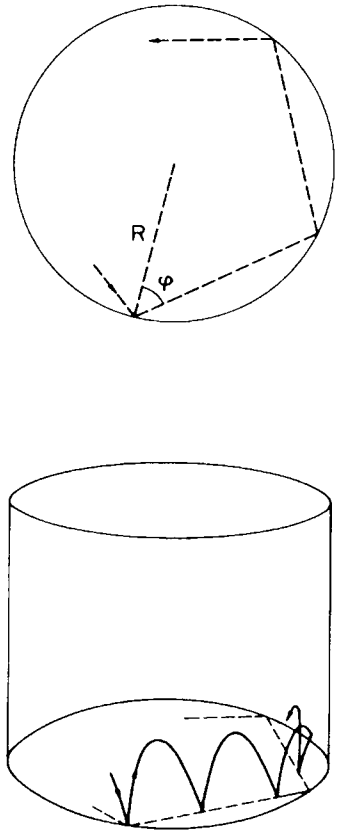

Fig. 10. Trajectory in a cylinder under influence of gravity.

5.3. RESULTS FOR CYLINDRICAL GEOMETRY INCLUDING THE EFFECTS OF GRAVITY

Calculations were carried out using numerical simulations of successive collisions according to eq. (A.7), for a number of collisions equivalent to 100 s measuring time. The total probability of detecting an $\bar{n}$ was calculated from eqs. (4.2) and (4.3) and integrated over energy (100 steps to a maximum energy of 1.8×10^{-7} eV), cos η (20 steps for cos η going from 0 to 1) and ϕ (5 steps from 0 to $\frac{1}{2}\pi$). Results for the total probability of detecting an $\bar{n}$ are shown in fig. 13 as a function of applied magnetic field. The orders of magnitude are similar to the results obtained for the spherical case without gravity.

The dependence on magnetic field is narrower in the cylindrical case reflecting the fact that the entire phase space below the $\bar{n}$ cut off is close to resonance around

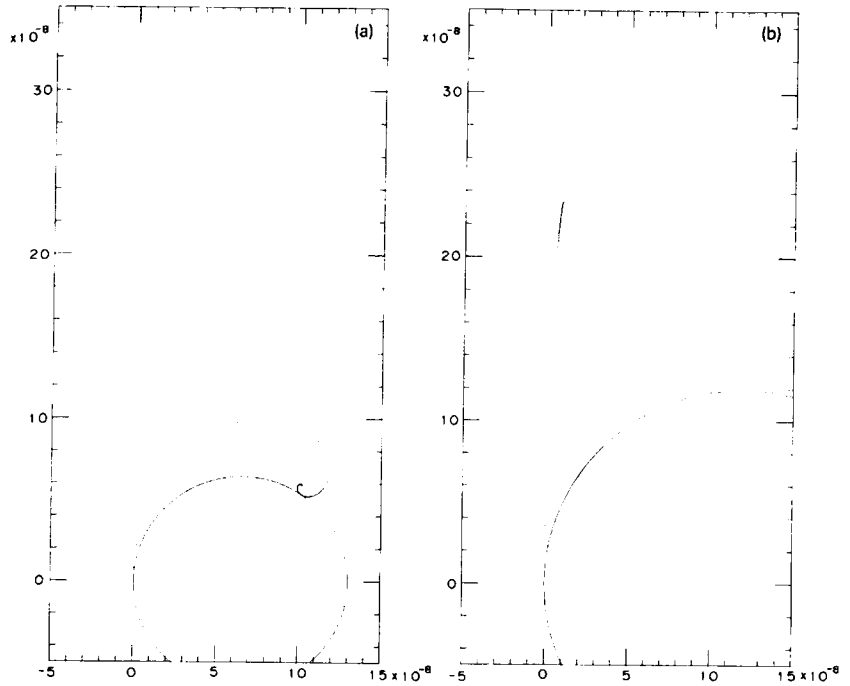

Fig. 11. Motion of the system point in the complex plane ($E=0.5\times10^{-8}$ eV, cos $\eta=0.25$, $\varphi=\frac{1}{4}\pi$, elapsed time = 100 s, ^{12}C diffuse potential, radius of cylinder $R=10\,000$ m (no side-wall collisions)). One point corresponds to 10 bounces, 0.5 s. The solid circle represents the free motion (no collisions at all). See text. ($\varepsilon=10^{-23}$ eV) (a) $B_0=1.30\times10^{-5}$ G, (b) $B_0=0.70\times10^{-5}$ G.

the field of 4×10^{-5} G (fig. 9a) for the diffuse potential and the peaks in the curves for the diffuse potential in fig. 13 are close to this value. However, the effect of the wall collisions in the cylinder reduces the value of the $\bar{n}$ probability as is seen in figs. 11 and 12.

6. Conclusion

Taking the potential between $\bar{n}$ and nucleus as being equal to that obtained from the strong interaction effects on $\bar{p}$-atom X-rays [14]) we have calculated the reflection properties of UC$\bar{N}$ from surfaces of ^{12}C and solid ^{16}O.

We then applied these results to a detailed study of the possibility of cancelling the effects of the UCN-$\bar{N}$ reflection phase shifts by applying an external magnetic field as was previously suggested by one of the present authors [7]). We find that, as expected, averaging over the phase space does substantially reduce the benefits of

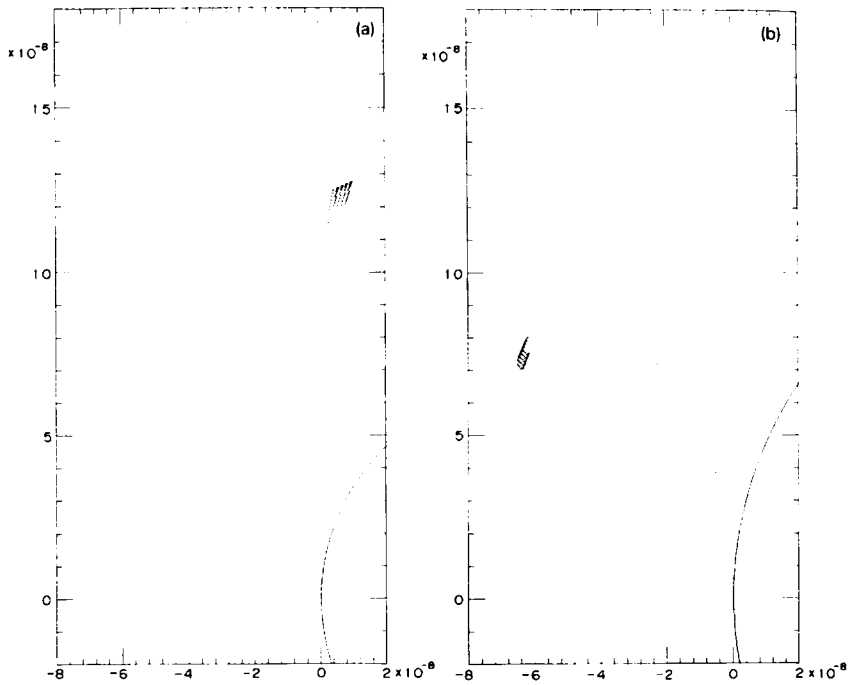

Fig. 12. As fig. 11 showing effect of wall collisions, $R = 0.3$ m. One point corresponds to 2 bounces, 0.1 s. See text. ($\varepsilon = 10^{-23}$ eV) (a) $B_0 = 1.30 \times 10^{-5}$ G, (b) $B_0 = 0.70 \times 10^{-5}$ G.

this cancellation, but there remains a significant enhancement with respect to the previously accepted idea that a single collision will destroy the coherence of the $\bar{n}$-wave function [5]). It should be noted that while our integrations have been carried out for the entire UCN energy spectrum up to the ^{12}C cut off in order to facilitate intensity estimates (UCN density figures are ususally quoted for the total spectrum up to the cut off), the enhancement mechanism is only effective for energies below the $\bar{n}$-cut off and for these energies the enhancement will be considerably larger than the averages presented here.

While UCN densities presently available (~ 50 UCN/cm^3) [17]) are such that the proposed quasi-free experiment [5]) is much more sensitive than anything that can even be contemplated with UCN, the situation could change with the introduction of more powerful sources, currently being planned [6,8,9]).

One of the authors (R.G.) would like to thank Prof. T. Nishikawa and other members of KEK and of Mombusho as well as the Society for the Promotion of Accelerator Physics for the hospitality extended during his visits to Japan.

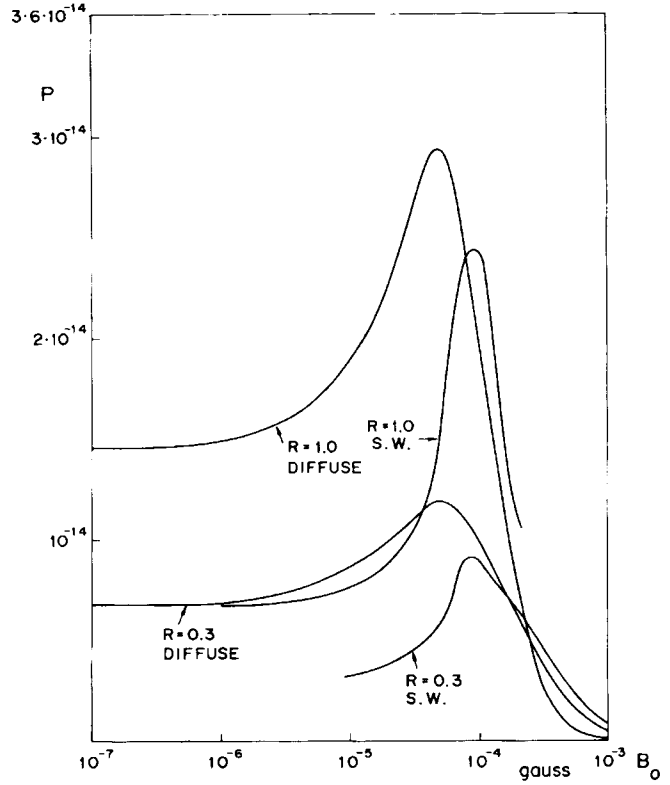

Fig. 13. Total probability of $\bar{n}$-annihilation in the first 100 s for a cylindrical container of ^{12}C including gravity versus applied magnetic field. ($\varepsilon = 10^{-23}$ eV).

Appendix A

Two circles of equal size, O, O', intersect at Q and U in fig. A.1. Take any point P on $\overline{QU}$. Choose S in such a way that $\overline{PS} = \overline{PQ}$. ($\angle$SPQ corresponds to the c.w. rotation angle α in the text. Note the perpendicular bisector of $\overline{QS}$ goes through P and O.) Take R in such a way that $\overline{QR} = \overline{QS}$. ($\angle$SQR is the c.c.w. rotation angle μ in the text.) Draw a circle R'RR'' from P. Then $\overline{QR'} = \overline{QR}$ because R' and R'' are symmetric with respect to $\overline{PO}$. Hence $\overline{R''S} = \overline{RQ}$. Hence $\Delta RQP \equiv \Delta R''SP$. Hence $\angle R''PS = \angle RPQ$.

In fig. A.1 $\overline{PQ}$ represents the line O-θ in fig. 1. We see from fig. A.1 that

$$\theta \sin(\tfrac{1}{2}\alpha) = R \sin\gamma, \tag{A.1}$$

($\gamma = \angle$QOP) where $R = \overline{OQ}$ = radius of the circle.

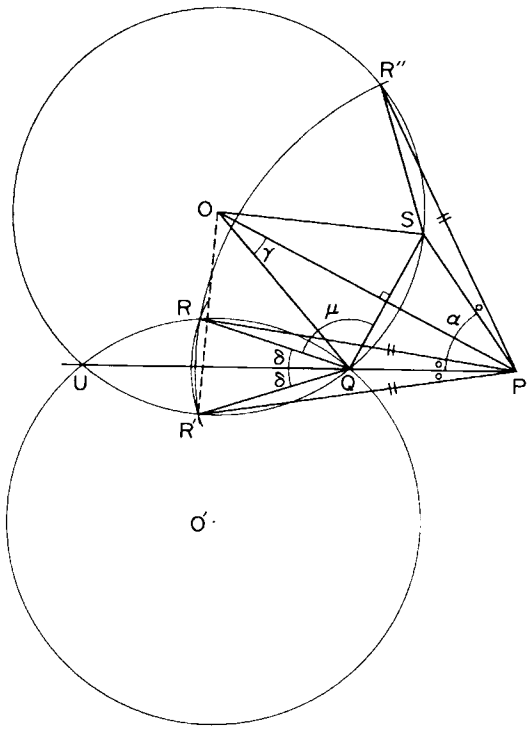

Fig. A.1. Geometry of motion in the complex plane (see appendix).

From ΔSQP: $\angle SQP = \frac{1}{2}(\pi - \alpha)$. Since $\overline{QR} = \overline{QS} = \overline{QR'}$,

$$\Delta OQS = \Delta OQR',$$

$$\angle OQS = \angle R'QO \equiv \lambda .$$

Hence

$$\angle R'QS = 2\lambda = 2\delta + \mu , \tag{A.2}$$

where $\delta = \angle RQU = \angle R'QU$. Now $\angle UQP = \pi$ so that

$$\delta + \mu + \tfrac{1}{2}\pi - \tfrac{1}{2}\alpha = \pi , \tag{A.3}$$

and $\gamma + \lambda = \frac{1}{2}\pi$.

Thus $\gamma = \frac{1}{2}\pi - \lambda = \frac{1}{2}\pi - \delta - \frac{1}{2}\mu$,

$$\gamma = \tfrac{1}{2}(\mu - \alpha) , \tag{A.5}$$

where we used (A.4),(A 3) and (A.2).

Further

$$R = \frac{\theta \sin \frac{1}{2}\alpha}{\sin \frac{1}{2}(\mu - \alpha)} , \tag{A.6}$$

using (A.5) and (A.1).

The next collision will rotate the system point (R in fig. A.1) to R''(i.e. rotation through α about P). We see that each collision results in the rotation of the system point by 2γ around each of the circles and the distance of the system point from the origin, Q, after n collisions will be $2R \sin(n\gamma)$. Thus the locus of the system is two circles for $\rho_{\bar{n}} = 1$, $\mu \neq \alpha$. (For $\rho_{\bar{n}} = 1$, $\mu = \alpha$, the circles degenerate into straight lines. Refer to fig. 8 of ref. [12]).)

Appendix B

Letting β_m equal the distance of the system point from the origin just before the mth collision (refer to fig. 7 of ref. [12])) we have

$$\beta_m = (\beta_{m-1} \rho \, e^{i\mu} - \theta) \, e^{-i\alpha} + \theta , \tag{A.7}$$

with $\beta_0 = 0$ as an expression of the sequence of steps (a), (b) and (c) following eq. (3.8). Note θ, α, μ and ρ are real. (θ is twice the usual mixing angle).

We can solve this recursion problem by forming the sum

$$\sum_{m=1}^{n} \rho^{n-m} \beta_m \, e^{i(n-m)(\mu-\alpha)}$$

$$= \sum_{m=1}^{n} \rho^{n-m+1} \beta_{m-1} \, e^{i(n-m+1)(\mu-\alpha)} + \rho^{n-m} \, e^{i(n-m)(\mu-\alpha)} \theta (1 - e^{-i\alpha}) , \tag{A.8}$$

using (A.7), and then cancelling common terms on both sides of (A.8). Thus we obtain eq. (13) of ref. [12]).

References

1) R. Golub and H. Yoshiki, Nucl. Phys. **A501** (1989) 869
2) R.N. Mohapatra and R.E. Marshak, Phys. Rev. Lett. **44** (1980) 1316
3) S. Marsh and K.W. McVoy, Phys. Rev. **D28** (1983) 2793
4) G. Fidecaro *et al.*, Phys. Lett. **B156** (1985) 122;
G. Puglierin, Nucl. Instr. Meth. **A284** (1989) 9
5) M. Baldo-Ceolin, National Bureau of Standard special publ. **711**; NBS Workshop on 'The investigation of fundamental interaction with cold neutron beams', ed. G.L. Greene (Gaithersburg, Maryland, 1985)
6) R. Golub and J.M. Pendlebury, Rep. Prog. in Phys. **42** (1979) 439;
A. Steyerl, Springer Tracts in Mod. Phys. **80** (1977) 57–201
7) H. Yoshiki, KEK reprint **80-10** (1980); Proc. ICANS-IV, KEK
8) R. Golub, Nucl. Instr. Meth. **226** (1984) 558, and references therein
9) H. Yoshiki, S. Ishimoto and M. Utsuro, Z. Phys. **B67** (1987) 161
10) R.A. Arndt, V.B. Prasad and Riazuddin, Phys. Rev. **D24** (1981) 1431

11) U.P. Trower and N. Zorhe, Phys. Rev. **D25** (1982) 3088
12) R. Golub, H. Yoshiki and R. Gähler, Nucl. Instr. Meth. **A284** (1989) 16
13) C.B. Dover, A. Gal and J.M. Richard, Phys. Rev. **D27** (1983) 1090, Phys. Rev. **C31** (1985) 1423;
C.J. Batty, Nucl. Phys. **A411** (1983) 399;
K.G. Chetyrkin, M.V. Kazarnovsky, V.A. Kuzmin and M.E. Shaposhnikov, Phys. Lett. **B99** (1981) 358
14) C.Y. Wong, A.K. Kerman, G.R. Satchler and A.D. Mackeller, Phys. Rev. **C29** (1984) 574
15) H. Feshbach, C.E. Porter and V.F. Weisskopf, Phys. Rev. **96** (1954) 448
16) L. Schiff, Quantum mechanics, 2nd edition (McGraw-Hill, New York, 1955);
M. Peshkin and G.R. Ringo, Am. J. Phys. **39** (1971) 324
17) A. Steyerl *et al.*, Phys. Lett. **A116** (1986) 347

Nuclear Physics **A536** (1992) 669–696
North-Holland

NUCLEAR PHYSICS A

QUARK MODELS OF NUCLEAR MATTER
(I). Basic models and ground-state properties

C.J. HOROWITZ

Nuclear Theory Center and Physics Department, Indiana University, Bloomington, IN 47405, USA

J. PIEKAREWICZ

Supercomputer Computations Research Institute, Florida State University, Tallahassee, FL 32306, USA

Received 17 June 1991

Abstract: Nuclear matter is modeled directly in the constituent quark coordinates. A many-body string flip potential is used which confines quarks, allows hadrons to separate and is symmetric in all quark coordinates. Variational Monte Carlo results are presented for the energy, wave function and quark correlation function of nuclear and quark matter for various densities. These show how quark clustering decreases with density. A percolation phase transition from nuclear to quark matter is observed which is characterized by a dramatic rearrangement of strings.

1. Introduction

In this paper we study some simple constituent quark models of nuclear matter. Here, uniform nuclear matter is modeled directly in the quark coordinates. Variational Monte Carlo results will be presented for a variety of ground-state properties at different densities.

The motivation for this study is threefold. First, we wish to examine the role of quark substructure in nuclear physics. For example, how are hadronic properties such as the nucleon form factor modified in the medium? By studying simple models, we hope to identify nuclear observables which may be sensitive to hadronic substructure.

Second, we will use these models (in later papers) to search for qualitatively new modes of excitation of many quark systems. These modes may be present in nuclei but they are not present in either single hadrons or hadronic models of nuclei. For example, there may be collective excitations of several quarks in a nucleus. These "quark giant resonances" could involve coherent density, spin, flavor or color oscillations of several quarks. In addition, the mixing between "quark-like" excitations, such as the nucleon to delta transition, and "hadronic" excitations, such as the Gamow–Teller resonance, can be examined.

One can also study the transition from nuclear to quark matter as the density increases. For example, how sharp is the transition? How does the color susceptibility change with density? What are useful observables which may provide signatures of the transition?

0375-9474/92/$05.00